Angular dependent ferromagnetic resonance analysis in a single micron sized cobalt stripe

C. Schoeppner,[1,a)] K. Wagner,[1,2] S. Stienen,[1,2] R. Meckenstock,[1] M. Farle,[1] R. Narkowicz,[3] D. Suter,[3] and J. Lindner[2]
[1]*Faculty of Physics and Center for Nanointegration Duisburg-Essen (CeNIDE), University of Duisburg-Essen, D-47057 Duisburg, Germany*
[2]*Helmholtz-Zentrum Dresden-Rossendorf, Institute for Ion Beam Physics and Materials Research, D-01328 Dresden, Germany*
[3]*Department of Physics, Technical University Dortmund, D-44221 Dortmund, Germany*

(Received 22 May 2014; accepted 6 July 2014; published online 17 July 2014)

We demonstrate how planar microresonators (PMRs) can be utilized to investigate the angular dependent magnetic resonance response of single magnetic nanostructures. In contrast to alternative detection schemes like electrical or optical detection, the PMR approach provides a classical means of investigating the high frequency dynamics of single magnetic entities, enabling the use of well-established analysis methods of ferromagnetic resonance (FMR) spectroscopy. To demonstrate the performance of the PMR-based FMR setup for angular dependent measurements, we investigate the microwave excited magnons in a single Co stripe of $5 \times 1 \times 0.02\,\mu m^3$ and compare the results to micromagnetic simulations. The evolution of excited magnons under rotation of one individual stripe with respect to a static magnetic field is investigated. Besides quasi uniform excitations, we observe magneto-static as well as localized excitations. We find a strong influence of inhomogeneous dynamic and static demagnetizing fields for all modes. © *2014 AIP Publishing LLC*. [http://dx.doi.org/10.1063/1.4890515]

I. INTRODUCTION

Since the dynamical magnetic properties determine the reversal as well as relaxation behaviour of the magnetization, the investigation of magnon excitations is of interest in the field of fundamental research as well as for modern spintronic applications.[1–3] The enlarged surface-to-volume ratio of nanostructures, inhomogeneous demagnetizing fields due to confined geometries, roughness, and morphology have considerable influence on magnetic properties and lead to complex magnetic excitations, which have been investigated, e.g., by means of Brillouin light scattering (BLS)[4,5] or recently by microstrip ferromagnetic resonance (FMR)[6] on arrays of stripes and dots. But integral measurements on array samples typically provide averaged signals due to the distribution of sizes, surface morphologies, and material parameters of the individual entities and are sensitive to disturbances due to inhomogeneous excitations. Hence, it is favorable to investigate magnonic excitations on an individual (single) nanoscale structure. Here, we focus on FMR, which is a powerful technique for the characterization of static and dynamic properties in magnetic solids.[7,8] Planar microresonators (PMR)[9] provide a sensitivity of $10^6\,\mu_B$ which allows the detection of excitation modes in a single Py stripe with size of $5.04 \times 0.59 \times 0.056\,\mu m^3$. So far PMR-FMR has been restricted to one fixed orientation of the sample to the externally applied magnetic field providing access to a magnetically hard or easy direction of a sample only.[10] To get access to anisotropic properties of individual nanosized samples, we extended the PMR technique to an angular dependent FMR experiment with high angular resolution covering the twofold symmetry of a stripe sample. The collective dynamics of a spin system can be expressed classically in a macrospin model by considering the excitation of the magnetization $\vec{M}$ in space and time, i.e., $\vec{M}(\vec{r},t)$. The time evolution of the magnetization $\vec{M}(\vec{r},t)$ driven by a continuous homogeneous microwave magnetic field $\vec{b}_{mw}$ at frequency $\frac{\omega}{2\pi}$ is described by the Landau-Lifshitz-Gilbert equation (LLG)[11] and the condition for resonant excitation, i.e., FMR can be calculated.

II. SAMPLE AND EXPERIMENTAL SETUP

The PMR as well as the Co stripe were produced by subsequent steps of electron beam lithography (EBL) in a scanning electron microscope (SEM) as described elsewhere.[10] The polycrystalline Co stripe $5 \times 1 \times 0.02\,\mu m^3$ with a 5 nm Pt capping is fabricated in the center of the PMR loop. The edges of the stripe are oxidized within a few Å, which is negligible in comparison to the micron sized width and length of the stripe. The polycrystalline Co shows a small in-plane magneto crystalline anisotropy of 5 mT measured on an extended thin film deposited as a reference in the same process. Furthermore, it shows a uniaxial out-of-plane anisotropy.[1] Both values are negligible in comparison to the shape anisotropy in this case. An SEM image of the PMR loop containing the Co stripe is shown in Fig. 1. The PMR's eigenfrequency was determined to be 14.23 GHz. Also shown in Fig. 1 is the coordinate system used throughout the paper.

PMRs utilize a linearly polarized high frequency magnetic field $\vec{b}_{mw}$ like conventional cavities but offer by four

a)Electronic mail: christian.schoeppner@uni-due.de

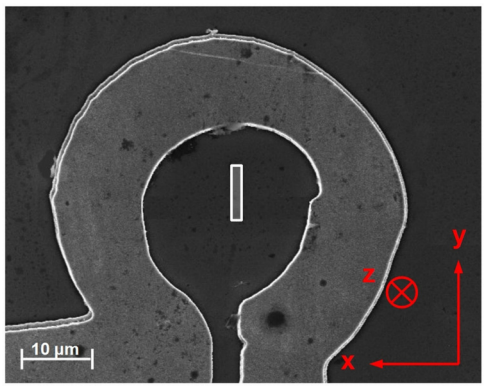

FIG. 1. SEM picture of the PMR loop containing as single Co stripe (highlighted by the grey rectangle) with dimensions $5 \times 1 \times 0.02\,\mu m^3$ (length- $\times$ width $\times$ thickness). The eigenfrequency of the PMR is 14.23 GHz with a quality factor = 14. The coordinate system shown in red is used throughout the paper. The PMR and the external magnetic field are in the x-y-plane and the microwave field $\vec{b}_{mw}$ is along the z-axis. The PMR is rotated within the x-y-plane during the angular dependent measurement, while B_{ext} is always applied in x-direction.

orders of magnitude increased sensitivity.[10] The sensitivity of the PMR is linked with an increased filling factor for the small stripe, which exceeds that of a conventional TE_{102} cavity at the 14 GHz operation frequency by a factor of 10^7. Nevertheless, due to the very small volume of the sample the absolute value of the filling factor for the stripe in PMR is comparable to that for a $5 \times 5 \times 0.0001$ mm^3 thin film sample in a classical cavity. The microresonator thus does not get overloaded by the sample. The microwave field generated inside the loop is always oriented along the z-axis, only in the vicinity of the microresonator edge ($<3\,\mu m$) the microwave field strongly increases and has non-negligible lateral components. The simulated microwave field in the microresonator has a concave meniscus-like shape open on the gap side.[9] In the PMR used in our experiments, the inhomogeneity of $\vec{b}_{mw}$ across the stripe is within 25% of its value in the center of the loop. In the extended setup angular dependent FMR experiments were performed at room temperature using a 14 GHz home-built spectrometer in cw modus.[12] The PMR containing the Co stripe was rotated in the x-y-plane in steps of 1° with respect to B_{ext} during the angular dependent measurement. The oscillator frequency of the spectrometer is stabilized by phase locked loop (PLL) with respect to a 10 MHz reference. As the PMRs are broadband, matching of the structure is not distorted by the thermal drift of the resonator frequency during the experiment. The static magnetic field B_{ext} was modulated with an amplitude of 2 mT at a frequency $f_m = 56$ kHz for lock-in detection and applied in the x-direction.

We performed micromagnetic simulations using the software package OOMMF[13,14] covering the experimentally investigated angular dependence. We extended the simulations in previous work with a locally resolved phase analysis of the magnetization with respect to $\vec{b}_{mw}$ to distinguish between resonantly driven and non-resonant oscillations. For this simulations, we considered a stripe of $5 \times 1 \times 0.02\,\mu m^3$, a damping parameter $\alpha = 0.006$, which is in agreement with literature[15–17] and a cw rf magnetic field applied along the z-axis. The cell size was chosen to 10 nm which is in the range of the exchange length and the exchange constant was chosen to 3×10^{-11} J/m. Anisotropy constants were set to zero. The small anisotropies measured on the reference sample were taken into account by means of a reduced magnetization of $M = 1130 \frac{kA}{m}$.

III. RESULTS

First, we will discuss the measured and simulated angular dependent FMR, followed by the analysis of the observed magnon modes separately for the long axis of the stripe parallel to B_{ext} (0°) and perpendicular to B_{ext} (90°), respectively.

A. The complete angular dependence

The results of the angular dependent measurement and simulation are summarized in Figs. 2(b) and 2(c), respectively, as a greyscale plot. On the horizontal axis, the in-plane angle is shown from 0° to 180°. The external field is represented on the vertical axis. In the greyscale plots (Figs. 2(b) and 2(c)), light grey color represents a positive sign for the signal amplitude while dark grey color represents negative ones. The FMR resonance field is found at a sharp contrast change from white to black color. Furthermore, the resonance fields for each in plane angle are highlighted by colored symbols. Different colors represent different types of excitations, which will be discussed later in detail. Every vertical line represents a single FMR spectrum as exemplary shown in Fig. 2(a)) for measurement and simulation. The red and blue line in the greyscale plot indicate spectra for 0° and 90° orientation, respectively, the spectra shown in (a) being recorded for the 90° orientation. Arrows indicate the position of the main resonance signal in both spectra and corresponding greyscale plot.

The angular dependent measurement reveals one major resonance signal (yellow), which exhibits a twofold symmetry as well as additional resonances at higher resonance fields ($B_{res}(\phi)$) for in-plane angles around 90°. For the major signal, we find $B_{res}(\phi = 90°) > B_{res}(\phi = 0°)$. The 90° orientation with the long axis of the stripe being perpendicular to the external field is the magnetically hard direction due to the shape anisotropy, while 0° represents the magnetically easy direction. Besides this main resonance, the simulation shows additional resonance signals of less intensity. For the angles close to the easy direction two resonance signals are observed in total ($B^1_{res}(\phi)$ and $B^2_{res}(\phi)$). For angles close to the hard direction at least four different resonance signals occur. Note that additional resonances appear with much smaller intensity and are magnified by a factor of 10 for better visualization in the greyscale plot. Taking a closer look at the evolution of $B^1_{res}(\phi)$ and $B^2_{res}(\phi)$ starting from the easy direction (0°) reveals that the two resonance modes approach each other when B_{ext} is rotated into the hard direction (90°). For in-plane angles around 60°, the two modes are energetically close, entering a strong coupling regime. The modes come closest around 62° and repel each other again at higher angles. This is supported by an intensity change of the main signal around 62° in Figs. 2(b) and 2(c). The rotational evolution of resonant modes, in general, and the observed

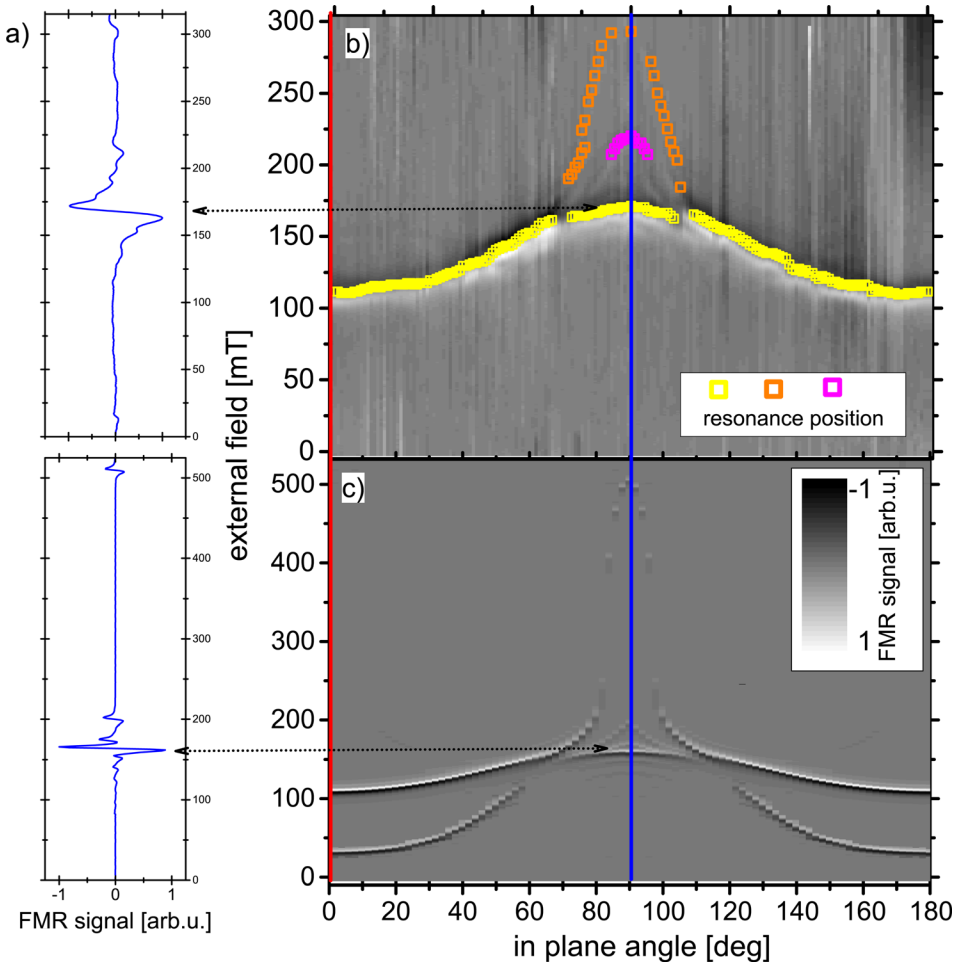

FIG. 2. Exemplary spectra and complete results of angular dependent FMR. (a) shows spectra for the hard direction in the measurement (top) and simulation (bottom). The vertical axis represents the external field, while the horizontal axis represents the normalized FMR signal. The angular dependence is shown in a greyscale plot for the measurement (b) and simulation (c). Horizontal axis: in plane angle of the external field. 0°: the stripes' long axis is parallel to the x-axis. Vertical axis: external magnetic field. Red and blue line: indicate the single spectra at 0° and 90° orientation. Color symbols show resonance positions taken from single spectra.

mode repulsion behaviour, in particular, is measured and visualized on a single magnetic stripe in an angular dependent FMR experiment. This demonstrates the potential of the improved PMR setup for the investigation of angular dependent magnetic resonance responses of single magnetic nanostructures. In Figs. 3(a) and 3(c), we present measured FMR spectra for the principal directions (0° and 90°). The corresponding simulated spectra are shown in Figs. 3(b) and 3(d).

The measured and simulated spectra are marked with (1)–(4) for the 0° configuration and (5)–(8) for 90°. The simulated spectra in Figs. 3(b) and 3(d) exhibit the same features as the measured ones and, moreover, the line positions of the major signals match very well (±1 mT). Only the measured mode (8) in 90° orientation has a significantly lower resonance field than the simulated one, which will be discussed later. The simulated spectra in Fig. 3 have a 6 mT narrower line width than in the experiment, which we attribute to extrinsic damping contributions in the experiment not accounted for by the α in the simulation. Due to the reduced linewidth, the individual resonance signals marked with (3), (4), (5), and (7) are more pronounced in the simulation. In order to investigate the nature of the magnon excitations, we use the simulation to visualize spatially resolved snapshots of the z-component of the precessing magnetization. Every snapshot depicts the magnetization orientation in each cell: arrows indicate the in-plane orientation averaged over 15 cells and color represents the z-component of the magnetization vector to be positive (red) or negative (blue). A color change from white to blue or red across the stripe indicates a phase shift of the precessing magnetization of adjacent cells. Note that for a resonantly excited precession a phase shift of $\frac{\pi}{2}$ between the magnetization and the driving field is present.

B. Magnetic field parallel to easy direction (0°)

In this part, the modes for the magnetic field being applied in the easy direction of the stripe are discussed. The corresponding spectra are shown in Figs. 3(a) and 3(b), while in Fig. 4 locally resolved snapshots of the magnetization are shown. Numbers (1)–(4) correspond to the resonance modes in the simulated spectra.

We start the discussion with resonance mode (2) in Fig. 4 since it is the main resonance in the spectrum. This mode is a quasi uniform excitation, where all magnetic moments precess in phase, but in contrast to a pure uniform mode it shows spatially varying amplitude. This can be seen from the color contrast which gradually decreases towards the sample edges. At the edges, an additional dynamic stray field is created which thus leads to a torque acting on the edge moments resulting in an effective pinning.[18] The resonance mode in snapshot (1) shows a color change across the width of the stripe. This implies a twofold phase shift of 180° of the dynamic component of magnetic moments. The

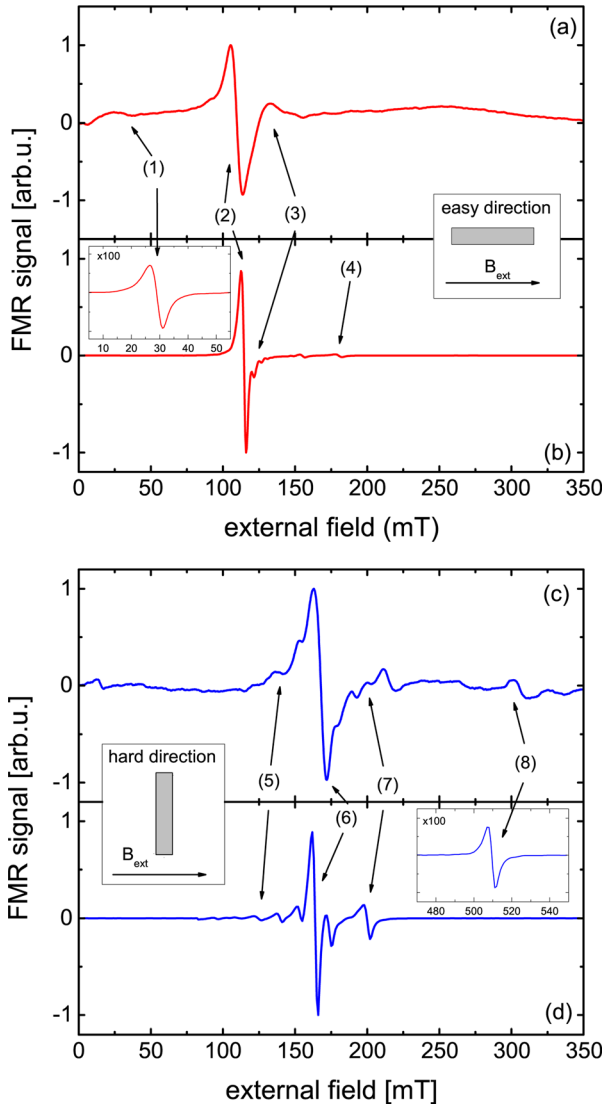

FIG. 3. Measured and simulated FMR spectra of the single Co stripe. (a) Measured spectrum for the easy direction. The stripes' long axis parallel to the x-axis and external field. (b) Simulated spectrum for the same orientation as (a). The inset shows resonance mode (1) at 36.5 mT and a magnification by a factor of 100. (c) Measured spectrum for the hard direction. The stripe's long axis parallel to the y-axis and perpendicular to the external field. (d) Simulated spectrum for the same orientation as (c). The inset shows the resonance mode (8) at 509 mT and a magnification by a factor 100. For a detailed description of the different excited modes, see text.

edge moments show no z-component due to the mentioned dipolar pinning at the sample. Excitation mode (1) is a dipolar and exchange coupled standing spin wave, with its wave vector $\vec{k}$ oriented perpendicular to the direction of the magnetization $\vec{k} \perp \vec{M}$.[19,20] To verify this, the micromagnetic simulation provides the possibility to analyze the phase relation between driving field b_{mw} and driven moments (Fig. 5(a)). We calculate the magnitude of both quantities with a time resolution of 1000 steps per oscillation (typically in the range of ps) for B_{ext} fixed at the resonance field. In Fig. 5(a), the phase relation is plotted for different locations along a line across the stripe. For all excited moments, the phase shift between b_{mw} and M_z is $\frac{\pi}{2}$, proving resonantly excited moments.

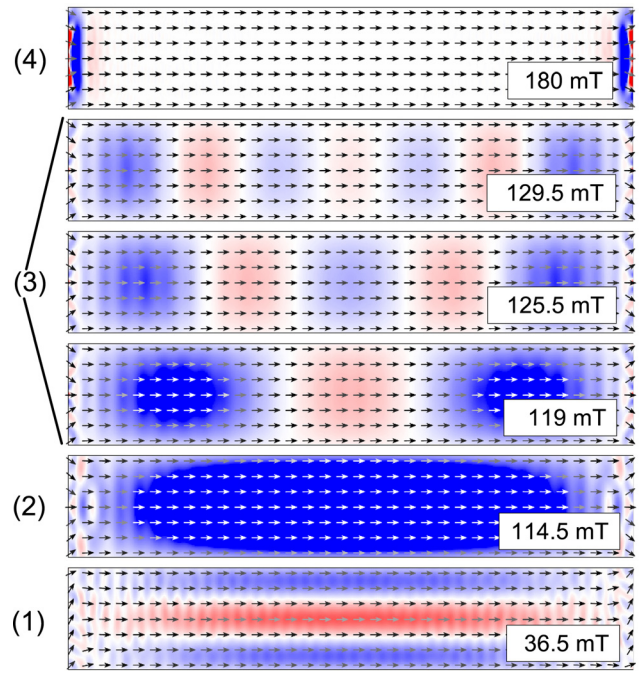

FIG. 4. Micromagnetic simulation: spatially resolved snapshots of the precessing magnetization for $\phi = 0$ at $B_{ext} = 36.5$ mT (1), 114.5 mT (2), 119 mT/125.5 mT/129.5 mT (3), and 180 mT (4). The numbers indicate the resonances in the spectra shown before. Arrows indicate the in-plane orientation of the magnetization averaged over 15 cells and color represents the out-of-plane component of the magnetization to be positive (red) or negative (blue).

At first glance resonance modes (3) appear to be spin waves as well but are of different nature. This can clearly be shown by the same phase analysis for b_{mw} and M_z as for mode (1) before. In Fig. 5(b), we show this phase analysis for relevant locations along the sample.

We find a phase shift between b_{mw} and M_z of about $\frac{\pi}{2}$ for the areas of highest color contrast (blue), while the low contrast area (red) reveals a phase shift of 0. Consequently, only those moments showing the most intense color in the snapshot are resonantly driven by the exciting microwave field. Moments appearing with low contrast are non-resonantly excited. Their precession is due to coupling only. The confinement of the sample leads to a strongly localized excitation and alters standing spin waves with $\vec{k} \parallel \vec{M}$, which are expected for higher field values[19] and still indicated by the snapshot. In the series of snapshots marked with (3), we observe the excitation being located closer to the edge of the sample with increasing strength of B_{ext}. Eventually, this leads to a strong localization at the edge of the sample as can be seen in snapshot (4).

C. Magnetic field parallel to hard direction (90°)

In this part, the modes for the magnetic field applied in the hard direction of the stripe are discussed. The spectra are shown in Figs. 3(c) and 3(d), while in Fig. 6 spatially resolved snapshots of the magnetization are presented. Here, numbers (5)–(8) correspond to the resonances in the spectra.

Applying the same phase analysis as for the modes in the easy direction mode (5) can be identified as a standing

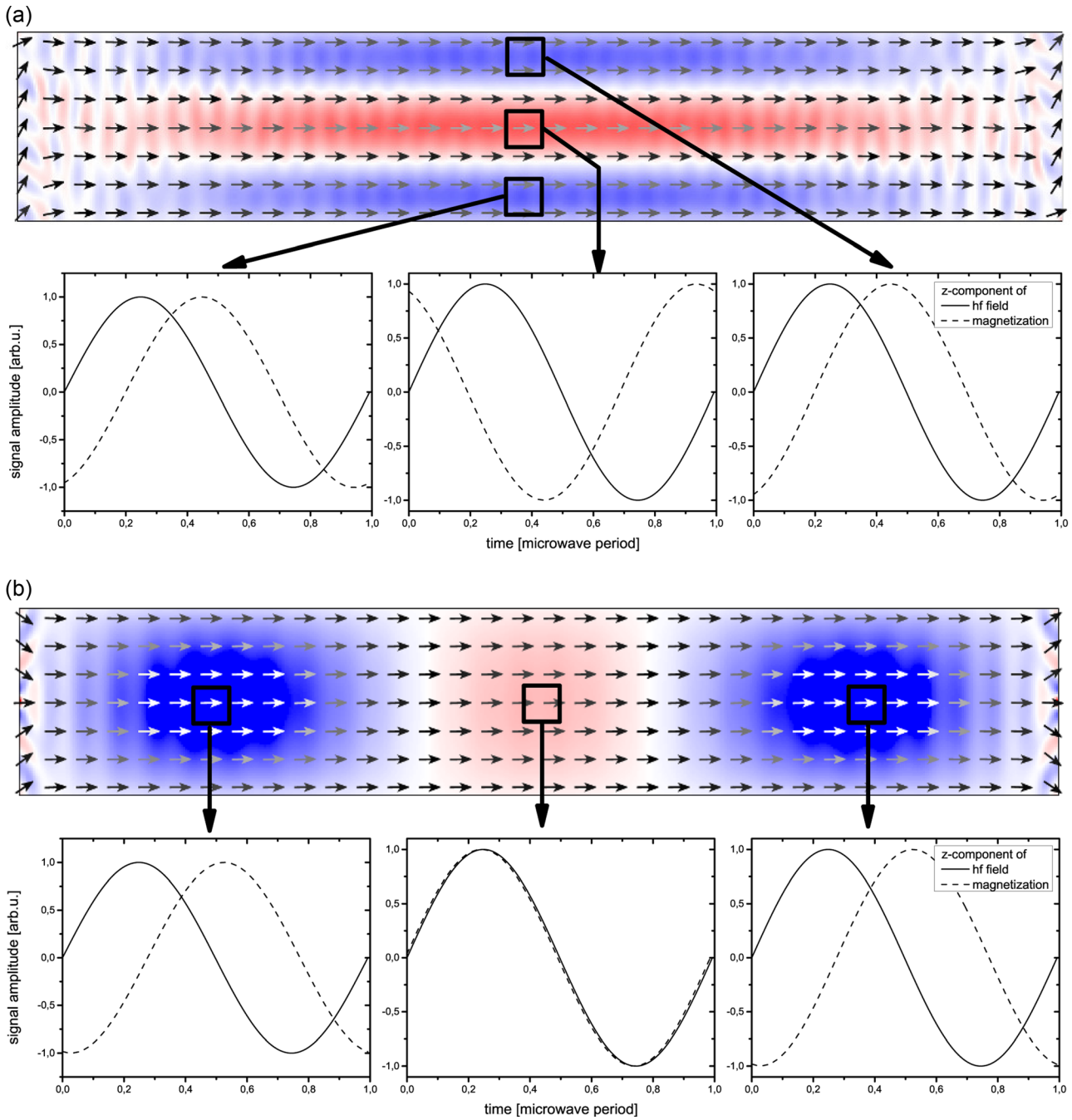

FIG. 5. Micromagnetic simulation: snapshots of the precessing magnetization for the principal direction 0°. (a) Visualizing a magnetization snapshot of mode (1) at 36.5 mT as before and the phase relation between exciting microwave field b_{mw} (solid line) and the precessing magnetization (dashed line). (b) Visualizing a magnetization snapshot of mode (3) at 119 mT as before and the phase relation between b_{mw} (solid line) and the precessing magnetization (dashed line). Magnitude of microwave field and magnetization are normalized to the respective maximum.

spin wave, with wave vector $\vec{k} \perp \vec{M}$.[19,20] Snapshot (6) shows that the quasi-uniform mode is much stronger localized for the magnetically hard direction due to an enhanced inhomogeneity of the static demagnetizing field along the short axis of the stripe. Since this inhomogeneity increases towards the edges the localization is enhanced in snapshots (7) and (8), depicting the resonance modes occurring at higher fields. The modes shown in snapshots (7) are localized excitations as discussed before for modes (3) in the easy direction in Figs. 4 and 5(b). Note, that for the hard direction, the edge moments are not aligned parallel with the external field so far. Eventually for a field value high enough, the edge moments are aligned parallel to the external field and the resonance condition is fulfilled for these moments only as depicted in snapshot (8). This edge mode occurs at a field value of 509 mT in the simulation but at a field value of approximately 300 mT in the experiment, see Figs. 3(c) and 3(d). This difference can be explained by the fact that the sample does not provide perfect edges as considered in the simulation. It has been shown, that edge roughness or a deviation of the edge surface angle from 90° may lead to an effective reduction of the edge saturation field.[21]

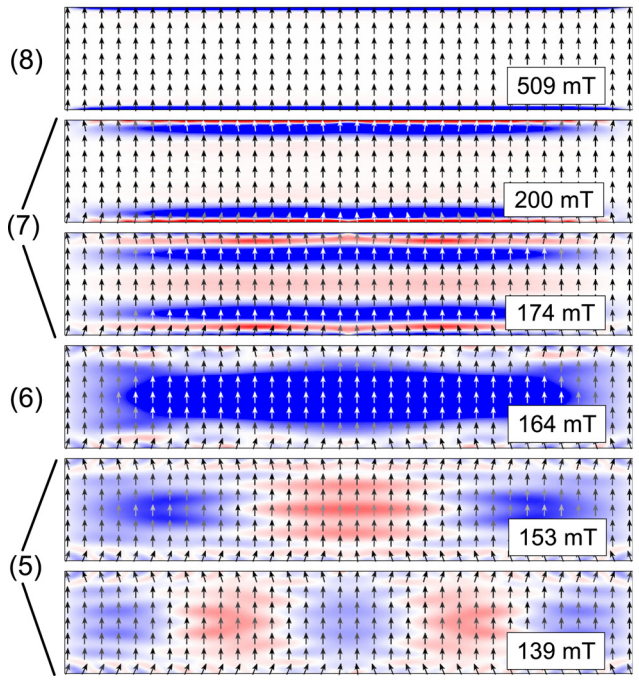

FIG. 6. Micromagnetic simulation: snapshots of the precessing magnetization for $\phi = 90$ at $B_{ext} = 139\,\text{mT}/153\,\text{mT}$ (5), 164 mT (6), 174 mT/200 mT (7), and 509 mT (8). The numbers indicate the marked resonance modes in spectra shown before. Snapshots depict the magnetization orientation as before.

IV. CONCLUSION

We studied the evolution of spinwave modes in a single Co stripe as a function of the orientation of an external magnetic field by FMR utilizing a planar microresonator and micromagnetic simulations with continuous wave excitation. In this analysis, we discuss the different observed magnon excitations and find excellent agreement between measured and simulated FMR spectra. In this particular case, even the quasi uniform mode is not a homogeneous excitation but appears localized due to the confinement of the sample. All modes with higher energy than this one show resonant excitation only in confined parts of the stripe. Eventually, this is maximal in a pure edge mode. The angular dependence reveals the evolution of the quasi uniform excitation for the easy direction into the pure edge mode for the hard direction in one excitation branch, which can be followed during the angular dependence. Furthermore, intermediate angles reveal mode repulsion of spinwave modes. Overall this shows the potential of highly sensitive PMR's to access anisotropic dynamic magnetic properties in individual nanosized samples with a high angular resolution. These investigations can be applied to samples provided by means of lithography and evaporation as shown here and utilized for potential spintronic applications as well as single nanoparticles.

ACKNOWLEDGMENTS

The authors thank Dr. Oliver Posth (VACOM GmbH, Jena, Germany) for strong support during sample preparation. Furthermore, we thank the DFG for financial support within program LI1567/3-1 and the Mercator Research Center Ruhr for financial support under Contract No. Pr-2011-0007.

[1]R. Meckenstock, I. Barsukov, O. Posth, and J. Lindner, "Locally resolved ferromagnetic resonance in cobalt stripes," Appl. Phys. Lett. **91**, 142507 (2007).
[2]M. Madami, S. Bonetti, G. Consolo, S. Tacchi, G. Carlotti, G. Gubbiotti, F. Mancoff, M. Yar, and J. Akermann, "Direct observation of a propagating spin wave induced by spin-transfer torque," Nat. Nanotechnol. **6**, 635–638 (2011).
[3]B. Lenk, H. Ulrichs, F. Garbs, and M. Münzenberg, "The building blocks of magnonics," Phys. Rep. **507**, 107–136 (2011).
[4]J. Jorzick, C. Krämer, S. Demokritov, B. Hillebrands, B. Bartenlian, C. Chappert, D. Decanini, F. Rousseaux, E. Cambril, E. Sondergard, M. Bailleul, C. Fermon, and A. Slavin, "Spin wave quantization in laterally confined magnetic structures," J. Appl. Phys. **89**, 7091–7095 (2001).
[5]Z. Wang, M. Kuok, S. Ng, D. Lockwood, M. Cottam, K. Nielsch, R. Wehrspohn, and U. Gösele, "Spin-wave quantization in ferromagnetic nickel nanowires," Phys. Rev. Lett. **89**, 027201 (2002).
[6]M. Kostylev, J. Ding, E. Ivanov, S. Samarin, and A. O. Adeyeye, "Microwave magnetic dynamics in highly conducting magnetic nanostructures," J. Appl. Phys. **115**, 173903 (2014).
[7]J. Lindner, R. Meckenstock, and M. Farle, "Applications of ferromagnetic resonance," in *Characterization of Materials* (John Wiley & Sons, Inc., 2002).
[8]M. Farle, T. Silva, and G. Woltersdorf, "Spin dynamics in the time and frequency domain," in *Magnetic Nanostructures*, edited by H. Zabel and M. Farle (Springer Tracts in Modern Physics, Springer, Berlin Heidelberg, 2013), Vol. 246, pp. 37–83.
[9]R. Narkowicz, D. Suter, and I. Niemeyer, "Scalling of sensitivity and efficiency in planar microresonators for electron spin resonance," Rev. Sci. Instrum. **79**, 084702 (2008).
[10]A. Banholzer, R. Narkowicz, C. Hassel, R. Meckenstock, S. Stienen, O. Posth, D. Suter, M. Farle, and J. Lindner, "Visualization of spin dynamics in single nanosized magnetic elements," Nanotechnology **22**, 295713 (2011).
[11]G. V. Skrotskii and L. V. Kurbatov, "Phenomenological theory of ferromagnetic resonance," in *Ferromagnetic Resonance*, edited by V. Vonsovskii (Pergamon Press, Oxford, 1966), pp. 12–77.
[12]R. Narkowicz, D. Suter, and R. Stonies, "Planar microresonators for EPR experiments," J. Magn. Reson. **175**, 275–284 (2005).
[13]See http://math.nist.gov/oommf/ contains the download of oommf software, as well as dokumentation and literature citing oommf.
[14]K. Wagner, S. Stienen, and M. Farle (submitted).
[15]H. Wijn, "1.1.2.10 g-factors and ferromagnetism resonance properties," in *Landoldt-Börnstein Database* (SpringerMaterials, 1986).
[16]J. Pelzl, R. Meckenstock, D. Spoddig, F. Schreiber, J. Pflaum, and Z. Frait, "Spin-orbit-coupling effects on g-value and damping factor of the ferromagnetic resonance in Co and Fe films," J. Phys.: Condens. Matter **15**, S451 (2003).
[17]B. Heinrich, J. F. Cochran, M. Kowalewski, J. Kirschner, Z. Celinski, A. S. Arrott, and K. Myrtle, "Magnetic anisotropies and exchange coupling in ultrathin fcc Co(001) structures," Phys. Rev. B **44**, 9348–9361 (1991).
[18]K. Y. Guslienko, S. O. Demokritov, B. Hillebrands, and A. N. Slavin, "Effective dipolar boundary conditions for dynamic magnetization in thin magnetic stripes," Phys. Rev. B **66**, 132402 (2002).
[19]C. Patton, "Magnetic excitations in solids," Phys. Rep. **103**, 251–315 (1984).
[20]R. Damon and J. Eshbach, "Magnetostatic modes of a ferromagnet slab," J. Phys. Chem. Solids **19**, 308–320 (1961).
[21]R. McMichael and B. Maranville, "Edge saturation fields and dynamic edge modes in ideal and nonideal magnetic film edges," Phys. Rev. B **74**, 024424 (2006).

Angular dependent ferromagnetic resonance analysis in a single micron sized cobalt stripe

C. Schoeppner, K. Wagner, S. Stienen, R. Meckenstock, M. Farle, R. Narkowicz, D. Suter, and J. Lindner

Citation: Journal of Applied Physics **116**, 033913 (2014); doi: 10.1063/1.4890515
View online: http://dx.doi.org/10.1063/1.4890515
View Table of Contents: http://scitation.aip.org/content/aip/journal/jap/116/3?ver=pdfcov
Published by the AIP Publishing